Geophysical Research Letters

RESEARCH LETTER
10.1029/2022GL100914

Key Points:

- A monthly index for the large-scale sea-surface temperature gradient of the separated Gulf Stream is presented
- Variations in the index throughout the year are related to atmospheric forcing
- Evidence of ocean-atmosphere feedback in the index is only apparent in wintertime

Supporting Information:

Supporting Information may be found in the online version of this article.

Correspondence to:

R. Parfitt,
rparfitt@fsu.edu

Citation:

Parfitt, R., Kwon, Y., & Andres, M. (2022). A monthly index for the large-scale sea surface temperature gradient across the separated Gulf Stream. *Geophysical Research Letters*, *49*, e2022GL100914. https://doi.org/10.1029/2022GL100914

Received 23 AUG 2022
Accepted 3 DEC 2022

Author Contributions:

Conceptualization: R. Parfitt, Y. Kwon
Formal analysis: R. Parfitt, Y. Kwon, M. Andres
Funding acquisition: R. Parfitt, Y. Kwon, M. Andres
Investigation: Y. Kwon
Methodology: Y. Kwon
Writing – original draft: R. Parfitt
Writing – review & editing: Y. Kwon, M. Andres

A Monthly Index for the Large-Scale Sea Surface Temperature Gradient Across the Separated Gulf Stream

R. Parfitt[1], Y. Kwon[2], and M. Andres[2]

[1]Department of Earth, Ocean and Atmospheric Science, Florida State University, Tallahassee, FL, USA, [2]Department of Physical Oceanography, Woods Hole Oceanographic Institution, Woods Hole, MA, USA

Abstract The strong sea-surface temperature (SST) gradient associated with the Gulf Stream (GS) is widely acknowledged to play an important role in shaping mid-latitude weather and climate. Despite this, an index for the GS SST gradient has not yet been standardized in the literature. This paper introduces a monthly index for the large-scale SST gradient across the separated GS based on the time-varying GS position detected from sea-surface height. Analysis suggests that the variations in the monthly average SST gradient throughout the year result primarily from SST variability to the north of the GS, with little contribution from SST to the south. The index exhibits a weak periodicity at ~2 years. Sea level pressure and turbulent heat flux patterns suggest that variability in the large-scale SST gradient is related to atmospheric (rather than oceanic) forcing. Ocean-to-atmosphere feedback does not persist throughout the year, but there is some evidence of wintertime feedback.

Plain Language Summary The Gulf Stream is a narrow and fast-flowing oceanic boundary current that transports warm tropical water north along the coast of Florida and out into the North Atlantic past Cape Hatteras. It is a region where sea-surface temperatures (SSTs) change dramatically over very short distances with much cooler temperatures on one side of the Gulf Stream (GS) (to the north) and warmer temperatures on the other side (to the south). This strong change in SST across the GS is important for weather systems that propagate in the Euro-Atlantic sector. Here, an index that measures how much the SSTs change with distance from month-to-month across the GS once it separates past Cape Hatteras is developed for the first time. It is found that variability in the index primarily results from SST variations to the north of the separated GS, which themselves are influenced by the atmosphere. There is evidence however that the SST variability represented by the index can also exert an influence on the atmosphere in wintertime. Additionally, the value of the index at any given time seemingly provides some information about the state of the index several years into the future.

1. Introduction

The important role of the Gulf Stream (GS) in modulating the mid-latitude atmosphere has been increasingly recognized in recent years. Studies have focused on the impacts both on the mean-state (e.g., Feliks et al., 2004) as well as on individual storm systems (e.g., Booth et al., 2012). In the time-mean, pronounced bands of near-surface wind convergence, anchored upward motion, and precipitation have been attributed to the strong sea-surface temperature (SST) gradients associated with the GS (e.g., Minobe et al., 2008, 2010). Studies also suggest a pronounced effect of the SST gradient on individual storm systems (e.g., Nakamura et al., 2004; Parfitt & Kwon, 2020).

Mechanisms pertaining to the role of the GS SST gradient in air-sea interaction are complex and vary extensively by region (i.e., over the topographically bound GS upstream of Cape Hatteras vs. over the separated GS). Wave-like GS meanders (evident as small-amplitude undulations in the SST gradient) propagate downstream along the South Atlantic Bight between Florida Straits and Cape Hatteras, with dominant periods less than 2 weeks (Andres, 2021) and larger amplitude, slower moving meanders grow downstream of the separation at Cape Hatteras (Lee & Cornillon, 1995). A strong SST gradient often coincides with the separated GS and extends far into the central North Atlantic. The position of the separated GS front itself also exhibits significant variability on monthly timescales (e.g., Andres, 2016). The weaker SST gradients associated with the topographically bound GS contribute significantly to the land-sea temperature contrast of the US east coast, which is known to be a critical ingredient of the North Atlantic storm-track (Brayshaw et al., 2009).

Furthermore, distinct air-sea interaction mechanisms have been linked to a broad range of spatiotemporal scales in SST gradients. For example, the "oceanic baroclinic adjustment" (Hotta & Nakamura, 2011; Taguchi et al., 2009), hypothesized to be a crucial component in maintaining baroclinicity in the mid-latitude storm track, is primarily associated with a large-scale SST gradient (like that spanning most of the separated GS ∼51°–75°W). Local and fine-scale SST gradients in the GS region have been shown to significantly influence diabatic frontogenesis in the lower atmosphere (Parfitt et al., 2016; Reeder et al., 2021).

Despite the importance of the SST gradient, most published indices focus on variability of GS position rather than the SST difference across the GS (Chi et al., 2021; Joyce et al., 2000; Peña-Molino & Joyce, 2008; Pérez-Hernández & Joyce, 2014; Taylor, 1996). To the authors' knowledge, an index tracking the observed (and moving) GS SST gradient has not been published. The purpose of this letter is to develop and introduce such an index for wider community use, and to use the index to examine drivers of the GS SST gradient and its role in North Atlantic air-sea interaction. To demonstrate the methodology and assess the usefulness of an observational index, the GS SST index initially developed here captures the large-scale SST gradient across the entire separated (rather than topographically bound) GS from the separation point near Cape Hatteras to ∼51°W, on a monthly timescale. As such, analysis focuses on month-to-month variability associated with the separated GS SST gradient.

The methods used to calculate the index are provided in Section 2. Drivers of the SST gradient index, as well as potential atmospheric impacts on a monthly timescale and the basic properties of the index time series, are investigated in Section 3. A discussion is provided in Section 4.

2. Data and Methods

The SST used in this study is from a high-resolution satellite-derived data set, the 0.25° National Oceanic and Atmospheric Administration Optimum Interpolation SST (NOAA OISST v2), primarily based on the Advanced Very High Resolution Radiometer measurement, which is available since September 1981 (Reynolds et al., 2007). The surface heat fluxes and sea level pressure (SLP) are taken from the European Centre for Medium-Range Weather Forecasts reanalysis 5 (ERA5, Hersbach et al., 2020), provided on a 0.25° longitude-latitude grid (native horizontal resolution ∼0.28°), since 1979. The time-varying monthly mean GS path is defined using the 25 cm isoline (e.g., Andres, 2016; Lillibridge & Mariano, 2013; Rossby et al., 2014) of the sea-surface height (SSH) from Copernicus Marine Service, provided at 1/4° resolution, from 1993 to 2019. The black line in Figure 1a illustrates this monthly mean GS path for December 1998 (along with the December 1998 average SST plotted in color). GS rings are excluded from the definition through identification of the longest contiguous isoline. Note that we use the GS path in each month of each year, rather than the climatological monthly mean paths. From each monthly mean GS path, a 'northern' region is defined from 0.5° to 3° latitude to the north for each longitude in the longitudinal range 51°–75°W (blue boundary). Similarly, a "southern" region is defined to the south (red boundary). In the event there is more than one latitude occupied by the GS path at a particular longitude (as at 65°W in Figure 1a), the northernmost (or southernmost) path latitude is used for the northern (southern) region definition. In the case that 3° latitude north of the GS at any given longitude is over land, the coastline is used as the border at that longitude. It is emphasized that the northern and southern regions are not fixed here due to the large monthly variability in GS path (Andres, 2016), although fixed regions may be sufficient for other current systems (e.g., Ohishi et al., 2016, 2017). Within each of these time-varying areas, the spatially averaged SST is calculated and the respective climatological monthly means for 1993–2019 are removed from each to obtain a northern and a southern SST anomaly. Subsequently, the large-scale separated GS SST gradient index value for any particular month in 1993–2019 is defined as the northern SST anomaly minus the southern SST anomaly. Negative (positive) values imply a stronger (weaker) GS SST gradient than usual for that particular month. Figures 1c and 1d show the time-series of the separated GS SST gradient index (color bars) with the time-series for the monthly SST anomalies averaged across the northern and southern regions respectively. The SST anomalies averaged across the northern and southern regions exhibit similar trends of 0.031 °Cyr^{-1} and 0.039 °Cyr^{-1} respectively, which nearly cancel such that the GS SST gradient index trend is only −0.008 °Cyr^{-1}. Seasonality of the GS SST index shows anomalies in the large-scale GS SST gradient from the long-term monthly means that are smaller in summer and fall than in winter and spring (Figure S1 in Supporting Information S1) Figure 1b illustrates the autocorrelation function of the GS SST gradient index time-series (Figures 1c and 1d), and is the subject of further discussion in Section 3.2.

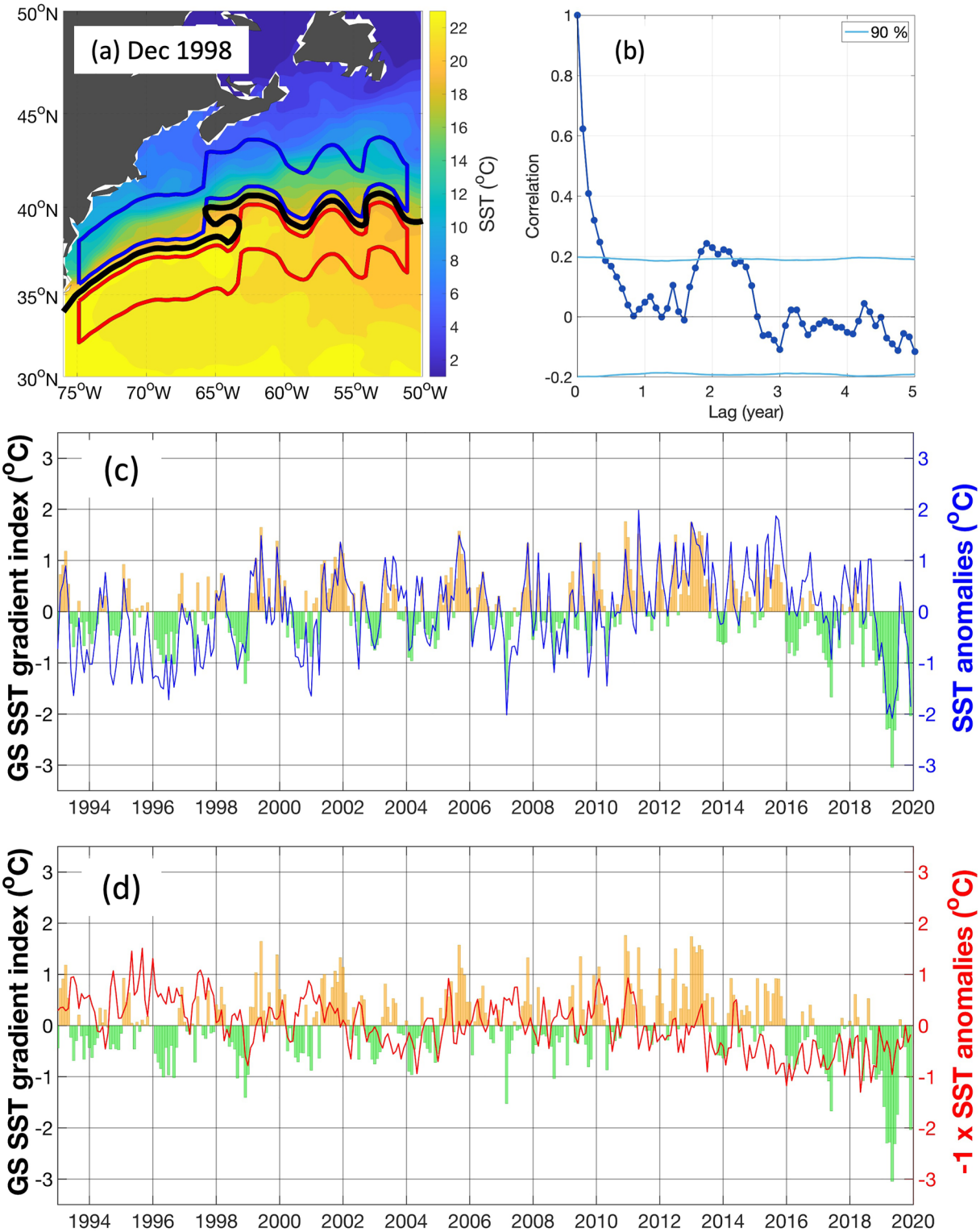

Figure 1. (a) The definitions of the regions for calculating the Gulf Stream (GS) sea-surface temperature (SST) gradient index, as defined for December 1998, with monthly average SST shown in color. The black line represents the monthly mean GS path based on the 25 cm isoline, the blue and red boundaries denote the northern and southern regions, respectively. (b) Autocorrelation function of the GS SST gradient index time series in (c–d). The light blue curves indicate statistical significance at 90%. (c) GS SST gradient index (color bars). Also shown in blue is the SST anomaly averaged over the northern region of the GS path. (d) As in (c), but with the SST anomaly averaged over the southern region shown in red. Note the time series for the southern region is multiplied by −1 to be consistent with the definition of the GS SST gradient index, and that the time series shown in (c–d) include their respective long-term linear trends.

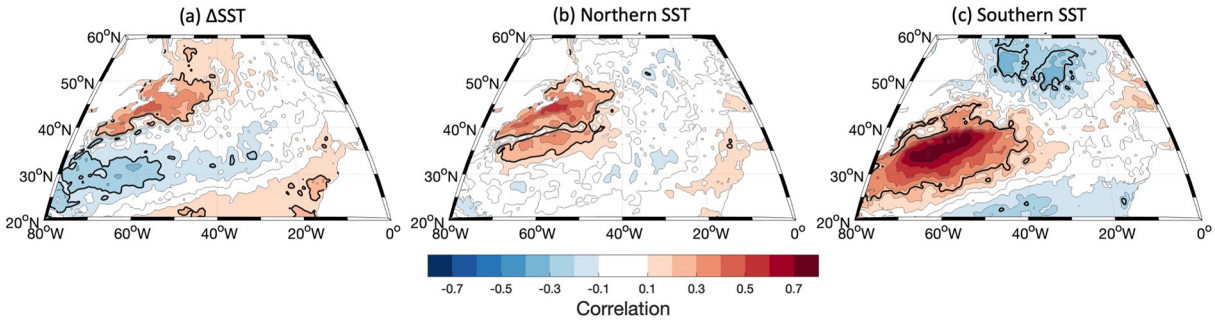

Figure 2. Correlation between monthly de-seasoned sea-surface temperature (SST) anomalies at each grid-point and (a) the Gulf Stream SST gradient index, (b) the SST averaged over the northern region, and (c) the SST averaged over the southern region. Black contours indicate statistical significance at 90%. All variables are detrended prior to calculating correlations.

3. Results

3.1. SST Structures Associated With the GS SST Gradient Index

With a monthly SST gradient index for the separated GS defined, that index is used to explore drivers of the monthly large-scale SST gradient, as well as the temporal behavior of the SST gradient itself. A natural first question relates to the SST structures that contribute to variability in the large-scale separated GS SST gradient. To address this, Figure 2a plots the simultaneous correlation between the SST gradient index and the monthly de-seasoned SST anomalies at each grid-point, with all variables detrended and de-seasoned prior to correlation analyses. Interestingly, a tri-pole pattern emerges across much of the North Atlantic, with positive correlations to the north of the GS, negative correlations further to the south ~30°N, and positive correlations in the eastern subtropical North Atlantic (although the positive correlations associated with this southern pole are barely statistically significant at 90%). The spatial extent of this correlation pattern suggests that variability in the SST gradient index is linked to large-scale forcing. Indeed, the leading empirical orthogonal function of North Atlantic SST, which is also a well-known SST tri-pole pattern, is associated with the North Atlantic Oscillation. The details of the tri-pole spatial structures, however, are not the same (Marshall et al., 2001), particularly in the GS region.

Notably, the region of significant negative correlation in Figure 2a occurs far south (~10°) of the time average separated GS position, and south of the GS meander envelope. The lack of correlation in the region directly south of the GS suggests that the primary SST signal driving the large-scale SST gradient is in fact associated with the region to the north of the GS. Correlations (after detrending and de-seasoning) between the monthly SST gradient index and the time-series of the monthly SST averaged over the northern and southern regions (e.g., Figure 1a) indeed confirm this—for the northern region it is 0.75, whereas for the southern region it is −0.17. In other words, a strengthening of the SST gradient results primarily from colder SST to the north of the GS. It is also noted that this strong co-variability between the SST gradient and the SST averaged across the northern region is strong on an annual time-scale as well—recalculating the correlation on yearly means still results in a correlation of 0.67. The SST anomalies averaged over the northern and southern regions are modestly correlated ($r = 0.44$).

For reference, Figure 2b illustrates the correlation between the monthly SST at each grid-point and the monthly SST averaged over the northern region. The signal is of single sign and primarily localized to the north of the GS, although a weaker signal of the same sign occurs to the south of the GS. Interestingly, the correlation vanishes along the narrow GS path, which suggests that the broad warm anomalies surrounding the GS may be forced by the atmosphere, while the SST along the GS itself may be driven by a separate oceanic process, such as the heat transport by the GS. Examination of the correlation between the monthly SST at each grid-point and the monthly SST averaged over the southern region (Figure 2c) demonstrates a basin-wide relationship, with the spatial structure highly reminiscent of that induced by fluctuations in the North Atlantic Oscillation (NAO; Cayan, 1992; Deser et al., 2010). It is noted that the correlation patterns in the southern regions in Figures 2a and 2c are not similar (whereas in the northern regions in Figures 2a and 2b, they are highly similar).

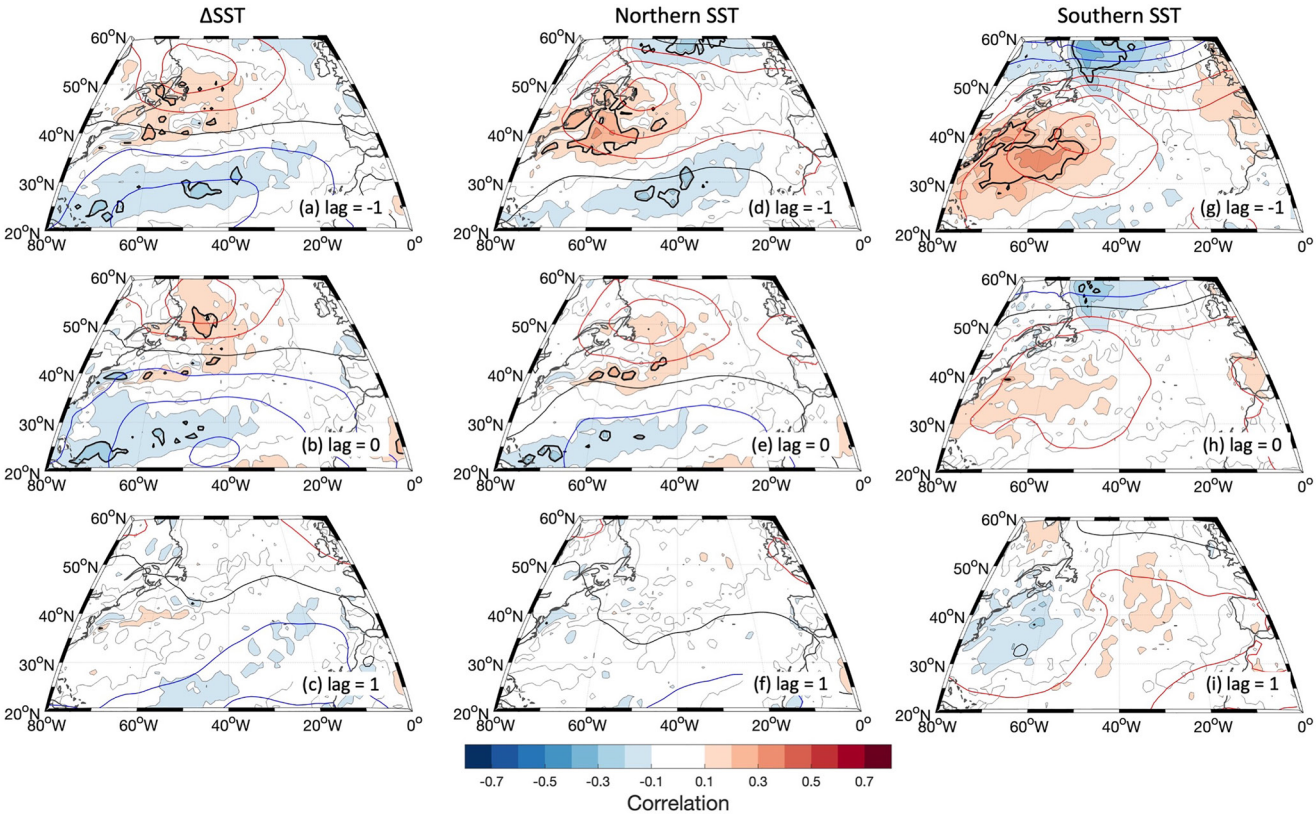

Figure 3. Correlation for the anomalies in the net surface heat flux (positive downward, color shading) and sea level pressure (SLP) (contours) against (a–c) the Gulf Stream sea-surface temperature (SST) gradient index (d–f) the SST anomalies averaged over the northern region, and (g–i) the SST anomalies averaged over the southern region. All variables are detrended prior to calculating correlations. The first row (a, d, g) is when the heat flux and SLP lead by 1 month. The second row (b, e, h) are simultaneous. The third row (c, f, i) is when the heat flux and SLP lag by 1 month. Thick black contours indicate statistical significance at 90% for heat flux correlations. The SLP correlations are statistically significant at 90% for correlations of 0.2 or higher. The thin red, blue and black contours indicate positive, negative, and zero correlations for SLP, with 0.1 interval.

3.2. Persistence of the GS SST Gradient Index

Next, we briefly examine whether the GS SST gradient index exhibits any temporal persistence. Accordingly, Figure 1b illustrates the autocorrelation of the GS SST gradient index. The autocorrelation exhibits a characteristic timescale of ∼5 months, consistent with typical SST persistence timescales in the mid-latitudes (Buckley et al., 2019; Bulgin et al., 2020). A statistically significant autocorrelation is also found at a lag of ∼2 years, indicating that processes driving the large-scale separated GS SST gradient may exhibit some degree of periodicity. One possibility could be a remote influence on the GS SST gradient of El Ninõ-Southern Oscillation (ENSO), which is known to impact North Atlantic SSTs directly to the north of the GS (Kwon et al., 2010; Rodríguez-Fonseca et al., 2016). However, while the autocorrelation of the time series associated with the northern region SSTs exhibits a similar peak at a lag of ∼2 years, it is not significant at 90% (Figure S2 in Supporting Information S1).

3.3. Role of the Atmosphere in the GS SST Gradient Index

The spatial structures of SSTs associated with the large-scale separated GS SST gradient, as well as those associated with the SSTs in the northern and southern regions were explored in Section 3.1. Lastly, we examine here how these SST structures are related to atmospheric variability. Figures 3a–3c illustrate correlations between the GS SST gradient index and anomalies (i.e., detrended and annual cycle removed) in both the SLP (contour) and net surface heat flux (positive downward, shading) at lags = −1, 0, +1 month (positive lag when the GS SST gradient index leads). Comparison of Figures 3a and 3b with Figure 2a indicates spatial coherence between heat flux anomalies and SST anomalies associated with variability in the GS SST gradient index. For positive values

of the GS SST gradient index, regions of increased heat flux into the ocean (i.e., positive anomalies) correspond with warmer SST and vice versa, indicating that the heat flux is driving the SST anomalies. The corresponding SLP anomalies exhibit high pressure anomalies over the subpolar gyre (Figure S3 in Supporting Information S1 shows a regression analysis of SLP with the GS SST gradient index)—the accompanying easterly anomalies between 40 and 50°N will act to reduce the strength of the overall westerlies, and thus the turbulent heat flux out of the ocean. These correlation patterns for the heat flux and SLP anomalies are strongest when the fields precede the GS SST index by 1 month (Figure 3a), and disappear when the GS SST index leads by 1 month (Figure 3c), which suggests forcing from atmospheric circulation variability on the GS SST index. This is consistent with the idea that an increase in low-pressure systems and associated atmospheric cold fronts will more frequently bring cold dry air over the GS region, resulting in increased heat loss from the upper ocean (Shaman et al., 2010). The lack of signal when the GS SST index leads by 1 month (Figure 3c) suggests no persistent ocean-atmosphere feedback via the large-scale separated GS SST gradient throughout the year, at least on a monthly timescale.

For completeness,Figures 3d–3f and 3g–3i illustrate analogous lead-lag composites, but for the SSTs averaged over the northern and southern regions, respectively. Similar patterns of heat flux and SLP variability are found in the relationship with the northern SSTs (Figures 3d–3f) as for the SST gradient index itself (Figures 3a–3c), though Figure 3d exhibits anomaly patterns shifted to the south. As such, the positive heat flux anomalies straddling the GS (Figure 3d) are consistent with broad warm SST anomalies to both the north and south of GS (Figure 2b). In addition, the lack of correlation with the heat flux in the narrow strip along the GS path (Figure 3d) is consistent with the lack of correlation with SST along the GS path (Figure 2b). This is also consistent with the results in Section 3.1, providing further evidence that the GS SST gradient index is primarily driven by SSTs in the northern region, which themselves are influenced by atmospheric forcing. For the SSTs in the southern region, Figure 3g again suggests that the SST variability is impacted by strong atmospheric forcing, which exhibits a north-south dipole similar to the NAO. Interestingly however, the absence of statistically significant correlations between heat flux anomalies and southern region SST anomalies at zero lag (Figure 3h) suggests the associated large-scale atmospheric forcing via air-sea heat exchange may not continue to persist once SST anomalies in the southern region have formed. This short duration during which heat fluxes determine southern region SSTs may be another potential factor in the primary importance of the northern SSTs for the GS SST gradient index. As for the GS SST gradient index, no evidence is found for a persistent ocean-to-atmosphere feedback via SSTs to the north or south of the GS throughout the year on a monthly timescale.

4. Discussion

A methodology for calculating the large-scale SST gradient of the separated GS on a monthly timescale has been developed. When all months of the year are considered, the large-scale SST gradient primarily results from SST variability to the north of the GS. These SSTs appear to be forced by atmospheric anomalies via changes in air-sea heat exchange. Analysis of the year 2019 (figures not shown) indicates this mechanism plays a role in setting the exceptionally strong large-scale GS SST gradient observed in that year, when the index exceeds −2°C (Figures 1c and 1d). Both SST and heat flux variability in the region north of the GS can also be influenced by warm core rings shed from the GS (e.g., Gangopadhyay et al., 2020; Silver et al., 2021). However, initial analysis suggests that no simple relationship exists between the number of warm core rings formed in a given month and the monthly SST anomalies averaged over the northern region nor between the number of rings and the SST gradient index (not shown). This lack of relationship underscores the importance of atmospheric forcing for monthly heat flux gradient changes associated with the large-scale separated GS SST gradient. In contrast, the SST along the GS itself appears to be driven by a distinct oceanic process (e.g., heat transport by the GS). This is consistent with recent studies highlighting that mesoscale SSTs and air-sea heat fluxes along the western boundary currents are generally ocean driven on monthly timescales (Bishop et al., 2017; Small et al., 2019). Furthermore, the GS SST gradient index appears to exhibit a statistically significant autocorrelation at ∼2 years. This might represent forcing from the Pacific through the impact of ENSO on SSTs to the north of the GS. Such a relationship could in theory provide statistical information regarding the likelihood of a strong large-scale separated GS SST gradient impacting the atmosphere years into the future.

Despite the recent literature documenting the importance of the large-scale separated GS SST gradient for weather and climate, no evidence is found here of a persistent impact on the atmosphere throughout the year. This is not necessarily surprising, as the large-scale separated GS SST gradient is significantly stronger in winter

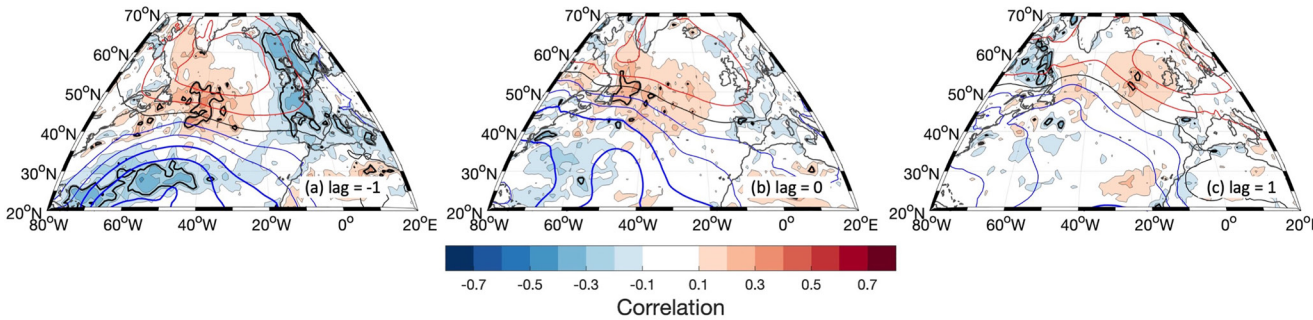

Figure 4. As in Figures 3a–3c, but for December–February only.

than it is throughout the rest of the year (Figure S1 in Supporting Information S1). Furthermore, in wintertime, atmospheric cold fronts are significantly more frequent and bring much colder and dryer air, leading to far greater air-sea heat exchanges in the GS region, both on average and in individual events. The average net turbulent heat flux in summertime is less than half it is in winter (Yu & Weller, 2007). Indeed, recalculation of Figure 3, but restricting correlations to just the December-February season illustrates much stronger correlations than when calculated for all the months (Figure 4). Furthermore, Figure 4c reveals statistically significant heat flux and SLP anomalies when the GS SST gradient index leads the atmosphere by 1 month. This suggests evidence of ocean-atmosphere feedback in wintertime that does not exist at other times of the year, that may contribute to increased persistence of monthly atmospheric SLP anomalies. Such a relationship has previously been observed by Ciasto and Thompson (2004) and Wills et al. (2016) using an index based on SST anomalies averaged over the GS region.

Several other avenues of research are natural extensions to this initial study of the large-scale SST gradient across the separated GS. It would be useful to perform a similar investigation into the SST gradient associated with the topographically bound GS to the south of the GS separation point near Cape Hatteras, as well as with the Mid-Atlantic Bight shelfbreak front to the north. This would aid in comparing the relative importance of surface temperature gradients at the land-sea boundary versus that across the separated GS front. Additionally, application of the method to the Kuroshio Extension would allow comparisons between the Pacific and Atlantic, although difficulties may arise from the complicated oceanic structure (e.g., Kida et al., 2016). It would also be interesting to explore the relationship between the GS SST gradient index and the latitudinal and path length variability of the GS, although preliminary analysis suggests no obvious co-variability on a monthly timescale (not shown). Application of an analogous methodology for daily timescales is also warranted, given that several studies have noted the importance of the GS SST gradient on daily timescales or shorter (Parfitt & Seo, 2018; Reeder et al., 2021). In relation to this last point, it may also be prudent to investigate whether the SST itself can be used to define such a GS SST gradient metric, which would provide the benefit of a longer record (1982-present for SST vs. 1993-present for SSH) and also all analysis would be limited to one data product. Indeed, atmospheric variability has been shown to vary significantly between data products because of differing SSTs (Masunaga et al., 2015, 2018; Parfitt et al., 2017). Lastly, the large-scale separated GS SST gradient index presented here captures only some of the fine-scale SST gradient variability along the GS (Figure S4 in Supporting Information S1), since the relatively broad regions used to define the index likely dampen much of the mesoscale SST variability. The development of indices to represent the local SST gradients across the GS region is critical, as many studies have indicated the significance of fine-scale turbulent heat flux gradients (e.g., Gentemann et al., 2020), that are present with sharp local SST gradients, for the development of atmospheric fronts and the associated circulation and precipitation (Jacobs et al., 2008; Parfitt et al., 2017). These avenues of research are currently underway.

Data Availability Statement

ERA5 (Hersbach et al., 2020) data can be freely obtained from the Climate Data Store (https://doi.org/10.24381/cds.adbb2d47). The NOAA OISST v2 data set (Reynolds et al., 2007) can be freely accessed at https://www.ncei.noaa.gov/products/optimum-interpolation-sst. Altimeter products can be accessed at https://marine.copernicus.eu/ by creating an account, then navigating to the ftp site my.cmems-du.eu, and select-

ing product "SEALEVEL_GLO_L4_MY_008_047." The GS SST gradient index, along with the code used to produce the index, will be made publicly available at https://www2.whoi.edu/staff/ykwon/data/.

Acknowledgments
The authors would like to thank ECMWF for allowing access to the ERA5 data set, NOAA for access to the NOAA OISST v2 data set, and the Copernicus Marine Service for access to the altimeter data. The authors would like to acknowledge discussions with Brian DeCicco, and the helpful comments of two anonymous reviewers. RP would like to gratefully acknowledge NSF OCE-2023585. Y-OK gratefully acknowledges NOAA MAPP NA21OAR4310341 and NSF AGS-2055236, and MA gratefully acknowledges NSF OCE-2122726. RP and Y-OK share equal contribution in lead authorship of this manuscript.

References

Andres, M. (2016). On the recent destabilization of the Gulf Stream path downstream of Cape Hatteras. *Geophysical Research Letters*, *43*(18), 9836–9842. https://doi.org/10.1002/2016gl069966

Andres, M. (2021). Spatial and temporal variability of the Gulf Stream near Cape Hatteras. *Journal of Geophysical Research: Oceans*, *126*(9), e2021JC017579. https://doi.org/10.1029/2021jc017579

Bishop, S. P., Small, R. J., Bryan, F. O., & Tomas, R. A. (2017). Scale dependence of midlatitude air–sea interaction. *Journal of Climate*, *30*(20), 8207–8221. https://doi.org/10.1175/jcli-d-17-0159.1

Booth, J. F., Thompson, L., Patoux, J., & Kelly, K. A. (2012). Sensitivity of midlatitude storm intensification to perturbations in the sea surface temperature near the Gulf Stream. *Monthly Weather Review*, *140*(4), 1241–1256. https://doi.org/10.1175/mwr-d-11-00195.1

Brayshaw, D. J., Hoskins, B., & Blackburn, M. (2009). The basic ingredients of the North Atlantic storm track. Part I: Land–sea contrast and orography. *Journal of the Atmospheric Sciences*, *66*(9), 2539–2558. https://doi.org/10.1175/2009jas3078.1

Buckley, M. W., DelSole, T., Lozier, M. S., & Li, L. (2019). Predictability of North Atlantic sea surface temperature and upper-ocean heat content. *Journal of Climate*, *32*(10), 3005–3023. https://doi.org/10.1175/jcli-d-18-0509.1

Bulgin, C. E., Merchant, C. J., & Ferreira, D. (2020). Tendencies, variability and persistence of sea surface temperature anomalies. *Scientific Reports*, *10*(1), 1–13. https://doi.org/10.1038/s41598-020-64785-9

Cayan, D. R. (1992). Latent and sensible heat flux anomalies over the northern oceans: Driving the sea surface temperature. *Journal of Physical Oceanography*, *22*(8), 859–881. https://doi.org/10.1175/1520-0485(1992)022<0859:lashfa>2.0.co;2

Chi, L., Wolfe, C. L., & Hameed, S. (2021). Has the Gulf Stream slowed or shifted in the altimetry era? *Geophysical Research Letters*, *48*(14), e2021GL093113. https://doi.org/10.1029/2021gl093113

Ciasto, L. M., & Thompson, D. W. (2004). North Atlantic atmosphere–ocean interaction on intraseasonal time scales. *Journal of Climate*, *17*(8), 1617–1621. https://doi.org/10.1175/1520-0442(2004)017<1617:naaioi>2.0.co;2

Deser, C., Alexander, M. A., Xie, S. P., & Phillips, A. S. (2010). Sea surface temperature variability: Patterns and mechanisms. *Annual Review of Marine Science*, *2*(1), 115–143. https://doi.org/10.1146/annurev-marine-120408-151453

Feliks, Y., Ghil, M., & Simonnet, E. (2004). Low-frequency variability in the midlatitude atmosphere induced by an oceanic thermal front. *Journal of the Atmospheric Sciences*, *61*(9), 961–981. https://doi.org/10.1175/1520-0469(2004)061<0961:lvitma>2.0.co;2

Gangopadhyay, A., Gawarkiewicz, G., Silva, E. N. S., Silver, A. M., Monim, M., & Clark, J. (2020). A census of the warm-core rings of the Gulf Stream: 1980–2017. *Journal of Geophysical Research: Oceans*, *125*(8), e2019JC016033. https://doi.org/10.1029/2019jc016033

Gentemann, C. L., Clayson, C. A., Brown, S., Lee, T., Parfitt, R., Farrar, J. T., et al. (2020). Fluxsat: Measuring the ocean–atmosphere turbulent exchange of heat and moisture from space. *Remote Sensing*, *12*(11), 1796. https://doi.org/10.3390/rs12111796

Hersbach, H., Bell, B., Berrisford, P., Hirahara, S., Horányi, A., Muñoz-Sabater, J., et al. (2020). The ERA5 global reanalysis. *Quarterly Journal of the Royal Meteorological Society*, *146*(730), 1999–2049. https://doi.org/10.1002/qj.3803

Hotta, D., & Nakamura, H. (2011). On the significance of the sensible heat supply from the ocean in the maintenance of the mean baroclinicity along storm tracks. *Journal of Climate*, *24*(13), 3377–3401. https://doi.org/10.1175/2010jcli3910.1

Jacobs, N. A., Raman, S., Lackmann, G. M., & Childs, P. P., Jr. (2008). The influence of the Gulf Stream induced SST gradients on the US East Coast winter storm of 24–25 January 2000. *International Journal of Remote Sensing*, *29*(21), 6145–6174. https://doi.org/10.1080/01431160802175561

Joyce, T. M., Deser, C., & Spall, M. A. (2000). The relation between decadal variability of subtropical mode water and the North Atlantic Oscillation. *Journal of Climate*, *13*(14), 2550–2569. https://doi.org/10.1175/1520-0442(2000)013<2550:trbdvo>2.0.co;2

Kida, S., Mitsudera, H., Aoki, S., Guo, X., Ito, S. I., Kobashi, F., et al. (2016). Oceanic fronts and jets around Japan: A review. *Hot Spots" in the Climate System*, 1–30.

Kwon, Y. O., Alexander, M. A., Bond, N. A., Frankignoul, C., Nakamura, H., Qiu, B., & Thompson, L. A. (2010). Role of the Gulf Stream and Kuroshio–Oyashio systems in large-scale atmosphere–ocean interaction: A review. *Journal of Climate*, *23*(12), 3249–3281. https://doi.org/10.1175/2010jcli3343.1

Lee, T., & Cornillon, P. (1995). Temporal variation of meandering intensity and domain-wide lateral oscillations of the Gulf Stream. *Journal of Geophysical Research*, *100*(C7), 13603–13613. https://doi.org/10.1029/95jc01219

Lillibridge, J. L., III, & Mariano, A. J. (2013). A statistical analysis of Gulf Stream variability from 18+ years of altimetry data. *Deep Sea Research Part II: Topical Studies in Oceanography*, *85*, 127–146. https://doi.org/10.1016/j.dsr2.2012.07.034

Marshall, J., Kushnir, Y., Battisti, D., Chang, P., Czaja, A., Dickson, R., et al. (2001). North Atlantic climate variability: Phenomena, impacts and mechanisms. *International Journal of Climatology: A Journal of the Royal Meteorological Society*, *21*(15), 1863–1898. https://doi.org/10.1002/joc.693

Masunaga, R., Nakamura, H., Kamahori, H., Onogi, K., & Okajima, S. (2018). JRA-55CHS: An atmospheric reanalysis produced with high-resolution SST. *Sola*, *14*(0), 6–13. https://doi.org/10.2151/sola.2018-002

Masunaga, R., Nakamura, H., Miyasaka, T., Nishii, K., & Tanimoto, Y. (2015). Separation of climatological imprints of the Kuroshio Extension and Oyashio fronts on the wintertime atmospheric boundary layer: Their sensitivity to SST resolution prescribed for atmospheric reanalysis. *Journal of Climate*, *28*(5), 1764–1787. https://doi.org/10.1175/jcli-d-14-00314.1

Minobe, S., Kuwano-Yoshida, A., Komori, N., Xie, S. P., & Small, R. J. (2008). Influence of the Gulf Stream on the troposphere. *Nature*, *452*(7184), 206–209. https://doi.org/10.1038/nature06690

Minobe, S., Miyashita, M., Kuwano-Yoshida, A., Tokinaga, H., & Xie, S. P. (2010). Atmospheric response to the Gulf Stream: Seasonal variations. *Journal of Climate*, *23*(13), 3699–3719. https://doi.org/10.1175/2010jcli3359.1

Nakamura, H., Sampe, T., Tanimoto, Y., & Shimpo, A. (2004). Observed associations among storm tracks, jet streams and midlatitude oceanic fronts. Earth's climate: The ocean–atmosphere interaction. *Geophysics Monograph*, *147*, 329–345.

Ohishi, S., Tozuka, T., & Cronin, M. F. (2017). Frontogenesis in the Agulhas return current region simulated by a high-resolution CGCM. *Journal of Physical Oceanography*, *47*(11), 2691–2710. https://doi.org/10.1175/jpo-d-17-0038.1

Ohishi, S., Tozuka, T., & Komori, N. (2016). Frontolysis by surface heat flux in the Agulhas return current region with a focus on mixed layer processes: Observation and a high-resolution CGCM. *Climate Dynamics*, *47*(12), 3993–4007. https://doi.org/10.1007/s00382-016-3056-0

Parfitt, R., Czaja, A., & Kwon, Y. O. (2017). The impact of SST resolution change in the ERA-Interim reanalysis on wintertime Gulf Stream frontal air-sea interaction. *Geophysical Research Letters*, *44*(7), 3246–3254. https://doi.org/10.1002/2017gl073028

Parfitt, R., Czaja, A., Minobe, S., & Kuwano-Yoshida, A. (2016). The atmospheric frontal response to SST perturbations in the Gulf Stream region. *Geophysical Research Letters*, *43*(5), 2299–2306. https://doi.org/10.1002/2016gl067723

Parfitt, R., & Kwon, Y. O. (2020). The modulation of Gulf Stream influence on the troposphere by the eddy-driven jet. *Journal of Climate*, *33*(10), 4109–4120. https://doi.org/10.1175/jcli-d-19-0294.1

Parfitt, R., & Seo, H. (2018). A new framework for near-surface wind convergence over the Kuroshio extension and Gulf Stream in wintertime: The role of atmospheric fronts. *Geophysical Research Letters*, *45*(18), 9909–9918. https://doi.org/10.1029/2018gl080135

Peña-Molino, B., & Joyce, T. M. (2008). Variability in the slope water and its relation to the Gulf Stream path. *Geophysical Research Letters*, *35*(3), L03606. https://doi.org/10.1029/2007gl032183

Pérez-Hernández, M. D., & Joyce, T. M. (2014). Two modes of Gulf Stream variability revealed in the last two decades of satellite altimeter data. *Journal of Physical Oceanography*, *44*(1), 149–163. https://doi.org/10.1175/jpo-d-13-0136.1

Reeder, M. J., Spengler, T., & Spensberger, C. (2021). The effect of sea surface temperature fronts on atmospheric frontogenesis. *Journal of the Atmospheric Sciences*, *78*(6), 1753–1771. https://doi.org/10.1175/jas-d-20-0118.1

Reynolds, R. W., Smith, T. M., Liu, C., Chelton, D. B., Casey, K. S., & Schlax, M. G. (2007). Daily high-resolution-blended analyses for sea surface temperature. *Journal of Climate*, *20*(22), 5473–5496. https://doi.org/10.1175/2007jcli1824.1

Rodríguez-Fonseca, B., Suárez-Moreno, R., Ayarzagüena, B., López-Parages, J., Gómara, I., Villamayor, J., et al. (2016). A review of ENSO influence on the North Atlantic. A non-stationary signal. *Atmosphere*, *7*(7), 87. https://doi.org/10.3390/atmos7070087

Rossby, T., Flagg, C. N., Donohue, K., Sanchez-Franks, A., & Lillibridge, J. (2014). On the long-term stability of Gulf Stream transport based on 20 years of direct measurements. *Geophysical Research Letters*, *41*(1), 114–120. https://doi.org/10.1002/2013gl058636

Shaman, J., Samelson, R. M., & Skyllingstad, E. (2010). Air–sea fluxes over the Gulf Stream region: Atmospheric controls and trends. *Journal of Climate*, *23*(10), 2651–2670. https://doi.org/10.1175/2010jcli3269.1

Silver, A., Gangopadhyay, A., Gawarkiewicz, G., Silva, E. N. S., & Clark, J. (2021). Interannual and seasonal asymmetries in Gulf Stream ring formations from 1980 to 2019. *Scientific Reports*, *11*(1), 1–7. https://doi.org/10.1038/s41598-021-81827-y

Small, R. J., Bryan, F. O., Bishop, S. P., & Tomas, R. A. (2019). Air–sea turbulent heat fluxes in climate models and observational analyses: What drives their variability? *Journal of Climate*, *32*(8), 2397–2421. https://doi.org/10.1175/jcli-d-18-0576.1

Taguchi, B., Nakamura, H., Nonaka, M., & Xie, S. P. (2009). Influences of the Kuroshio/Oyashio extensions on air–sea heat exchanges and storm-track activity as revealed in regional atmospheric model simulations for the 2003/04 cold season. *Journal of Climate*, *22*(24), 6536–6560. https://doi.org/10.1175/2009jcli2910.1

Taylor, A. H. (1996). North–south shifts of the Gulf Stream: Ocean-atmosphere interactions in the North Atlantic. *International Journal of Climatology: A Journal of the Royal Meteorological Society*, *16*(5), 559–583. https://doi.org/10.1002/(sici)1097-0088(199605)16:5<559::aid-joc26>3.0.co;2-z

Wills, S. M., Thompson, D. W., & Ciasto, L. M. (2016). On the observed relationships between variability in Gulf Stream sea surface temperatures and the atmospheric circulation over the North Atlantic. *Journal of Climate*, *29*(10), 3719–3730. https://doi.org/10.1175/jcli-d-15-0820.1

Yu, L., & Weller, R. A. (2007). Objectively analyzed air–sea heat fluxes for the global ice-free oceans (1981–2005). *Bulletin of the American Meteorological Society*, *88*(4), 527–540. https://doi.org/10.1175/bams-88-4-527

[Geophysical Research Letters]

Supporting Information for

A monthly index for the large-scale sea surface temperature gradient across the separated Gulf Stream

R.Parfitt[1] and Y.Kwon[2], M. Andres[2]

[1]Department of Earth, Ocean and Atmospheric Science, Florida State University, Tallahassee, FL
[2]Department of Physical Oceanography, Woods Hole Oceanographic Institution, Woods Hole, MA

Contents of this file

Figures S1 to S4

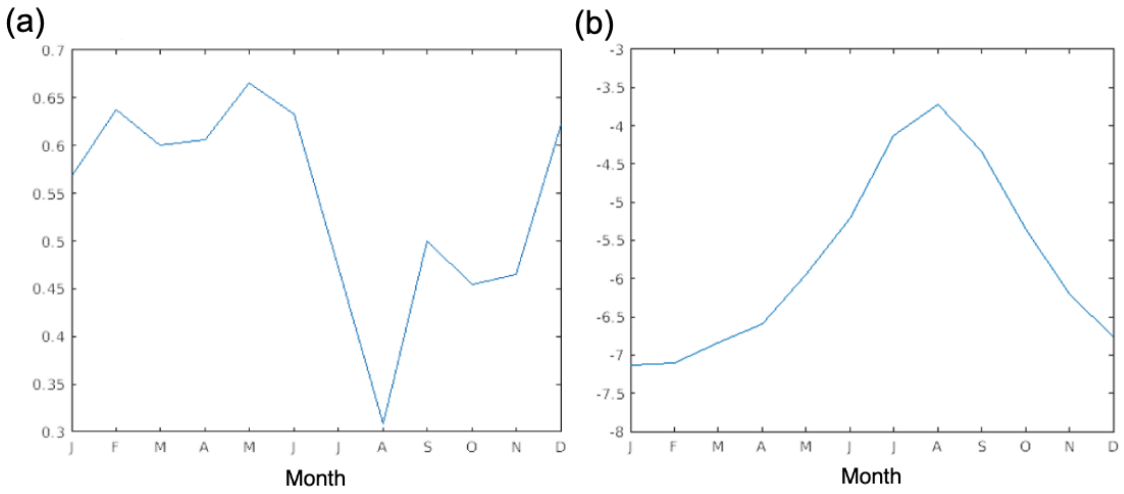

Figure S1. (a) The monthly means of the absolute values of the de-seasoned GS SST gradient index in Figures 1c-d. (b) The monthly means of the difference in SSTs averaged over the northern and southern regions in Figure 1a (northern minus southern), without de-seasoning the SSTs prior to the subtraction. The values correspond directly to the average magnitude of the large-scale GS SST gradient in any given month, with more negative values indicating a stronger large-scale GS SST gradient.

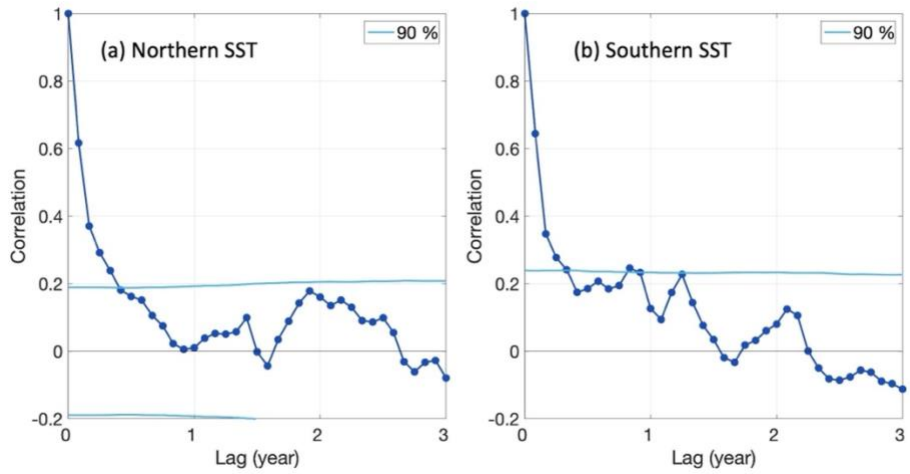

Figure S2. Autocorrelation function of the time series for the monthly SST anomalies averaged over the (a) northern (Figure 1c) and (b) southern region (Figure 1d). The light blue curves indicate statistical significance at 90%.

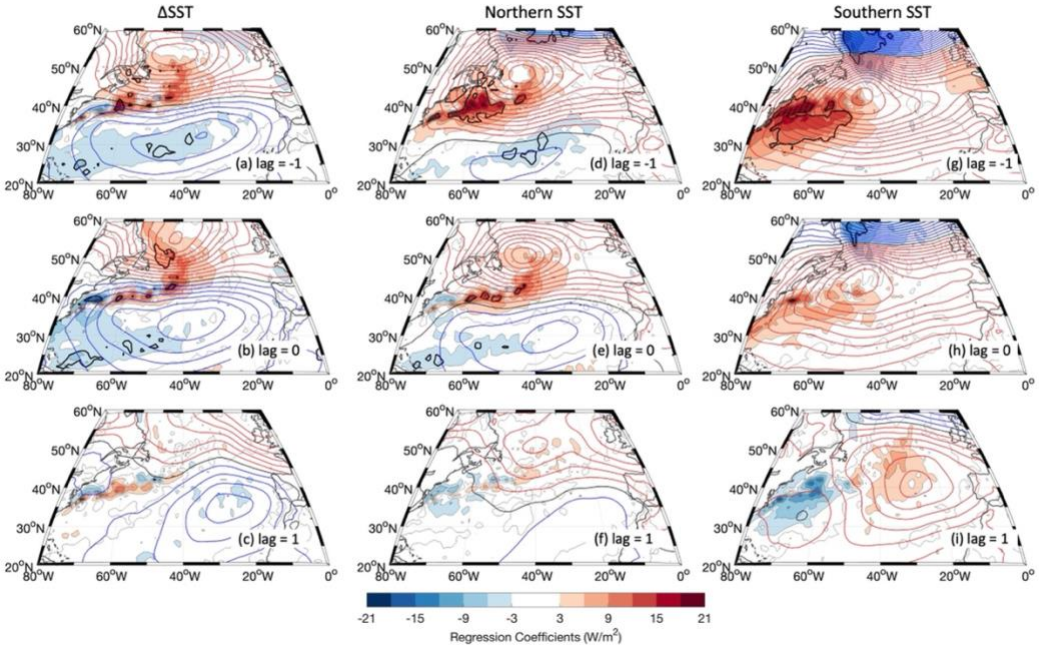

Figure S3. As in Figure 3, but showing regression instead of correlation. Regression coefficients for the net surface heat flux are shown in color, while those for SLP are plotted in contours (contour interval 0.1hPa).

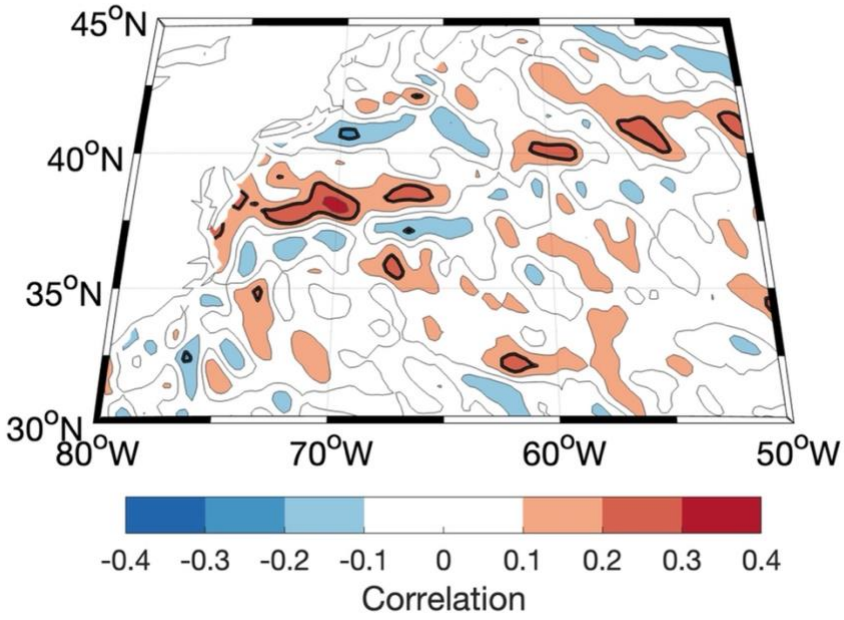

Figure S4. Simultaneous correlation between monthly de-seasoned local SST gradient anomalies at each grid-point and the large-scale GS SST gradient index. Yellow contours indicate statistical significance at 90%.